

Pattern Formation and Coarse-Graining in Two-Dimensional Colloids Driven by Multiaxial Magnetic Fields

Kathrin Müller,[†] Natan Osterman,[‡] Dušan Babič,[§] Christos N. Likos,[⊥] Jure Dobnikar,^{*,||,#} and Arash Nikoubashman^{*,○}

[†]Institute of Complex Systems: Theoretical Soft Matter and Biophysics, Forschungszentrum Jülich, Wilhelm-Johnen-Straße, 52428 Jülich, Germany

[‡]Department of Complex Matter and ^{||}Department of Theoretical Physics, Jožef Stefan Institute, Jamova 39, 1000 Ljubljana, Slovenia

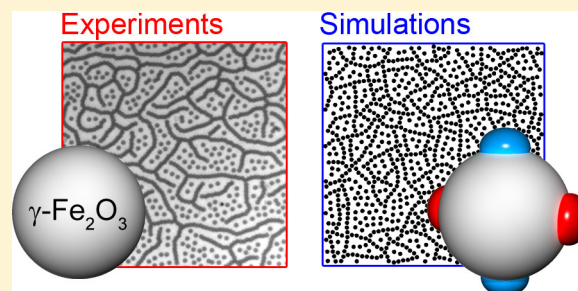
[§]Department for Mathematics and Physics, University of Ljubljana, Jadranska 19, 1000 Ljubljana, Slovenia

[⊥]Faculty of Physics, University of Vienna, Boltzmannngasse 5, A-1090 Vienna, Austria

[#]Department of Chemistry, University of Cambridge, Lensfield Road, CB2 1EW Cambridge, U.K.

[○]Department of Chemical and Biological Engineering, Princeton University, Princeton, New Jersey 08544, United States

ABSTRACT: We study the pattern formation in a two-dimensional system of superparamagnetic colloids interacting via spatially coherent induced interactions driven by an external precessing magnetic field. On the pair level, upon changing the opening angle of the external field, the interactions smoothly vary from purely repulsive (opening angle equal to zero) to purely attractive (time-averaged pair interactions at an opening angle of 90°). In the experiments, we observed ordered hexagonal crystals at the repulsive end and coarsening frothlike structures for purely attractive interactions. In both of these limiting cases, the dense colloidal systems can be sufficiently accurately described by assuming pairwise additivity of the interaction potentials. However, for a range of intermediate angles, pronounced many-body depolarization effects compete with the direct induced interactions, resulting in inherently anisotropic effective interactions. Under such conditions, we observed the decay of hexagonal order with the concomitant formation of short chains and percolated networks of chains coexisting with free colloids. In order to describe and investigate these systems theoretically, we developed a coarse-grained model of a binary mixture of patchy and nonpatchy particles with the ratio of patchy and nonpatchy colloids as the order parameter. Combining genetic algorithms with Monte Carlo simulations, we optimized the model parameters and quantitatively reproduced the experimentally observed sequence of colloidal structures. The results offer new insight into the anisotropy induced by the many-body effects. At the same time, they allow for a very efficient description of the system by means of a pairwise-additive Hamiltonian, whereupon the original, one-component system features a two-component mixture of isotropic and patchy colloids.



1. INTRODUCTION

Colloids constitute most soft materials and biological systems and are characterized by coexisting length and time scales giving rise to complex many-body interactions and a rich diversity of self-assembled structures.^{1–14} Besides their obvious technological importance, they are frequently seen as model systems for studying the fundamental relationship between interactions at the particle level and macroscopic organization or self-assembly. In order to understand the macroscopic properties of such systems theoretically, it is tempting to replace the many-body interactions with effective pairwise additive forces. Such a mapping cannot be exact: the form of the effective interactions depends on the route in which they were extracted, and they are typically density-dependent or even state-dependent, which might limit their practical use.^{15,16} Nevertheless, when these restrictions are properly accounted

for, the reduction is very rewarding since it leads to an enormous simplification of the original problem.

A particularly interesting case of colloids with tunable interactions is superparamagnetic colloids. These particles carry no magnetic dipole moment in the absence of an external magnetic field, but they feature a high effective magnetic susceptibility of $\chi_{\text{eff}} \cong 10^{-11} \text{ A m}^2/\text{T}$ due to doping with a ferromagnetic core (usually $\gamma\text{-Fe}_2\text{O}_3$).¹⁷ Thus, a weak external field \mathbf{B} induces a magnetic moment $\mathbf{m} = \chi_{\text{eff}}\mathbf{B}$ on the colloids perfectly aligning with the former; here, magnetic moment fluctuations can be ignored.^{17,18} In the case of superparamagnetic colloids, the physical interactions are induced by external magnetic fields and the mutual depolarization

Received: March 7, 2014

Revised: April 16, 2014

effects lead to complex many-body interactions and rich phase behavior. Unlike most other colloidal interactions, magnetic interactions are not mediated by the suspending medium, which hugely simplifies their theoretical description (as compared to, for example, charged colloids) and makes magnetic colloids a clean model for many-body systems. Accordingly, superparamagnetic colloids have been employed to study self-assembly and two-dimensional phase transitions both under static^{17–25} and under rotating^{26–34} external magnetic fields.

The subject of this paper is the two-dimensional (2D) assembly of superparamagnetic colloids. The spatially coherent induced colloidal interactions are driven by an external magnetic field that precesses around an axis perpendicular to the plane on which the colloids lie. These interactions can be efficiently controlled by the geometry of the field, i.e., by the opening angle θ of the cone on which the latter is precessing. Depending on the opening angle, the induced interactions range from simple pairwise additive dipolar repulsions at small angles $\theta \approx 0$, interactions with short-range attraction and long-range repulsion with pronounced many-body effects at intermediate values of $45^\circ \lesssim \theta \lesssim 60^\circ$, and peculiar spatially isotropic van der Waals-like interactions at the so-called magic angle $\theta_m \approx 54.7^\circ$ to pairwise additive dipolar attraction at large $\theta \approx 90^\circ$. The interactions between two isolated colloids are always isotropic in the plane of confinement; however, at certain angles θ the many-body terms introduce an effective anisotropy that results in the formation of chains when more than two colloids are present.^{27,35,36} The observed morphology in the experiments ranges from hexagonal crystals at small θ to a mixture of crystals and short chains to percolated chains coexisting with pockets of free colloids to frothlike structures coarsening due to purely attractive forces at large θ . On the basis of the rich behavior observed in the experiments and on the character of the many-body effects, we constructed a coarse-grained model: a mixture of patchy and nonpatchy colloids with anisotropic effective interactions. We combine Monte Carlo and genetic algorithm methods to extract optimal parameter values for the effective interactions. By varying the composition ratio of patchy vs nonpatchy particles, we are able to reproduce the structural properties of the system quantitatively for opening angles of $0 < \theta < \theta_m$.

The rest of the article is organized as follows. In section 2, we describe the experimental setup and techniques, and we give an overview of the experimental results. In section 3, we describe theoretically many-body interactions due to depolarization effects, bringing forward the complexity of the problem and the necessity to design an effective pairwise-additive system that accounts for the richness of the experimental results. This inverse-engineering procedure is described in section 4, where it is also demonstrated that it brings forward excellent agreement with experimental results both for structure and dynamics. Finally, in section 5 we summarize and draw our conclusions, whereas some technical aspects regarding the genetic algorithm approach employed in the inverse engineering are relegated to the Appendix.

2. EXPERIMENTS

In the experiments, we studied the behavior of a suspension of superparamagnetic colloidal spheres with a diameter of $\sigma = 1.05 \mu\text{m}$ (Dynabeads, MyOne Carboxy; dissolved in Dynabeads solution to prevent sticking) enclosed between two coverslips, confining the colloids to two spatial dimensions. The time-dependent external

magnetic field was applied by three orthogonal pairs of Helmholtz coils as depicted in Figure 1(a).

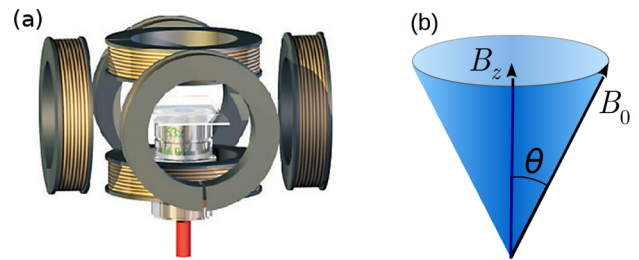


Figure 1. (a) Sample cell and surrounding pairs of Helmholtz coils. (b) Total external magnetic field precessing on a cone with opening angle θ .

In the absence of the external magnetic field, the colloids were arranged in a random configuration, which served as the initial condition for the experiments. Initially, the static magnetic field $\mathbf{B}_z = B_0 \hat{z}$ with magnitude $B_0 = 2.5 \text{ mT}$ was switched on, inducing repulsive dipolar interactions and a hexagonal colloidal arrangement. We then simultaneously decreased the perpendicular static component and increased the orthogonal rotating component of the field, while keeping the magnitude B_0 of the magnetic field constant. The external field thus precessed on a cone with an opening angle θ [see Figure 1(b)]:

$$\mathbf{B}_{\text{ext}} = B_0 \begin{pmatrix} \sin \theta \cos \omega t \\ \sin \theta \sin \omega t \\ \cos \theta \end{pmatrix} \quad (1)$$

The induced magnetic moments on the colloidal particles follow the external field, and ideal colloids should not physically rotate. We used a high rotational frequency of $2\pi\omega \approx 400 \text{ Hz}$ for the magnetic field so that the field variations were much faster than the typical translational and rotational relaxation times of the colloid, which are on the order of a few tens of seconds. Under these assumptions, the effect of the driving field on the colloids is well captured by the time-averaged values of the field. However, due to pinning defects and shape anisotropy the constantly rotating external field exerts a small net torque on the colloids, resulting in physical rotation with a smaller frequency. Physical rotation would imply hydrodynamic currents and additional complex interactions in the system. Moreover, since the net rotation can be of the same order as the colloidal relaxation times, the time-averaged fields would not be sufficient to describe the system and kinetic synchronization effects may become important.^{26,33} In this work, we wanted to prevent such complex interactions and study only the effects of time-averaged magnetic induced interactions. Therefore, we switched the direction of the field precession every 360° to suppress the net rotation of the colloidal particles.²⁷

By increasing the relative magnitude of the rotating component of the magnetic field, we slowly varied the opening angle θ from zero to 90° , and as epitomized in Figure 2, we observed distinct colloidal patterns: for small θ values, crystalline structures with hexagonal symmetry were stable. At around $\theta = 45^\circ$, a fraction of colloids assembled into short chains, which grew longer with increasing θ and eventually formed a percolating network coexisting with free colloids. The amount of free colloids vanished entirely near the magic angle of $\theta_m \approx 54.7^\circ$,²⁷ beyond which frothlike structures were observed. In the experiments, we kept the conditions at each θ constant for a sufficiently long time, i.e., several minutes, in order to ensure that a steady state had been reached. Self-assembled structures emerged in less than 10 s, and the systems fully settled within 120 s. The mixture of percolating and free colloids appeared to be stable: once formed, it did not evolve over the time of the experiment. Beyond θ_m , the interactions are purely attractive, and the frothlike structures slowly coarsened in the course of the experiment.

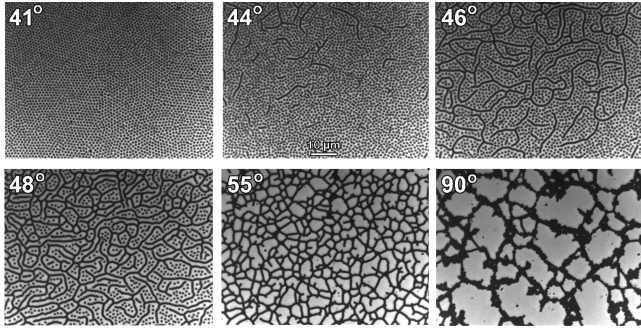


Figure 2. Patterns observed in the experiments at various opening angles θ of the external magnetic field with magnitude $B_0 = 2.5$ mT. The two-dimensional density of the colloidal particles is the same for all snapshots and equals $\rho\sigma^2 = 0.33$.

3. MANY-BODY INDUCED INTERACTIONS

The peculiar behavior observed in the experiment is due to the complex nature of the induced magnetic interactions among the colloids. The local field at the position of each colloid i is the sum of the external precessing magnetic field and the dipolar contributions of all other colloids in the system, $\mathbf{B}_{\text{loc}}(\mathbf{r}_i, t) \equiv \mathbf{B}_{\text{ext}}(t) + \sum_{j \neq i} \mathbf{B}_j(\mathbf{r}_{ij}, t)$ with $\mathbf{r}_{ij} \equiv \mathbf{r}_i - \mathbf{r}_j$. The local field determines the induced dipoles $\mathbf{m}_i(t)$

$$\mathbf{m}_i(t) = \frac{\pi\sigma^3}{6\mu_0} \chi_m (\mathbf{B}_{\text{ext}}(t) + \sum_{j \neq i} \mathbf{B}_j(\mathbf{r}_{ij}, t)) \quad (2)$$

where χ_m denotes the magnetic susceptibility of the material³⁷ and the prefactor expresses the aforementioned effective magnetic susceptibility of the colloids,

$$\chi_{\text{eff}} \equiv \frac{\pi\sigma^3}{6\mu_0} \chi_m \quad (3)$$

which is, evidently, a size-dependent quantity. The field induced by the j th colloid at the position of the i th colloid is then given by

$$\mathbf{B}_j(\mathbf{r}_{ij}, t) = \frac{\mu_0}{4\pi} \frac{3(\mathbf{m}_j(t) \cdot \hat{\mathbf{r}}_{ij})\hat{\mathbf{r}}_{ij} - \mathbf{m}_j(t)}{r_{ij}^3} \quad (4)$$

where $\hat{\mathbf{r}}_{ij} = \mathbf{r}_{ij}/|\mathbf{r}_{ij}|$. Equations 2 and 4 must be solved self-consistently.

The emerging colloidal interactions are inherently many-body, i.e., the energy $E(\{\mathbf{r}_i\})$ of any given configuration of colloids $\{\mathbf{r}_i\}$ depends on the positions of all colloids in the system. In particular, it is given by the time average over the period of the field revolution:

$$E = -\frac{1}{2} \sum_{i=1}^N \langle \mathbf{m}_i(t) \cdot \mathbf{B}_{\text{loc}}(\mathbf{r}_i, t) \rangle \quad (5)$$

where $\langle O(t) \rangle \equiv (1/\tau) \int_{\tau} dt O(t)$ is the average of an arbitrary, time-dependent quantity $O(t)$ over a period τ of the rotation of the external field and the sum runs over all N particles in the system. To demonstrate the many-body nature of the interactions, let us consider a simple system of three colloidal particles in the precessing external field and compare the energy of two close-packed configurations of these three colloids in the xy plane: a chain with energy $E_{\text{ch}}(\mathbf{r}_1, \mathbf{r}_2, \mathbf{r}_3)$ and an equilateral triangle $E_{\text{tr}}(\mathbf{r}_1, \mathbf{r}_2, \mathbf{r}_3)$. Let us build up the system one by one: the

dipole moment induced on an isolated colloid in the external field is $m_0 = \chi_{\text{eff}} B_0$ and its energy is $E_1 = -1/2 m_0 B_0 \equiv -1/2 E_0$. The pair potential $V(|\mathbf{r}_1 - \mathbf{r}_2|) \equiv V(r_{12})$ for two isolated colloidal particles separated by a distance r is obtained by solving eqs 2–5 for the pair and subtracting twice the energy of an isolated colloid, $V(r_{12}) \equiv E(\mathbf{r}_1, \mathbf{r}_2) - E_0$. The resulting two-body interaction takes fully into account the mutual depolarization effects of the two particles and is purely repulsive with $V(r) \propto r^{-3}$ at $\theta = 0$ and then develops a short-range attraction (while maintaining the long-range repulsion) with increasing θ until it becomes completely attractive at the magic angle θ_m with $V(r) \propto -r^{-6}$ (see ref 27 for more details). Upon further increasing $\theta \rightarrow 90^\circ$, the potential crosses over to a $V(r) \propto -r^{-3}$ dependence. The evolution from $\theta = 0$ to 90° is shown in the upper row of Figure 3. We evaluated the energies

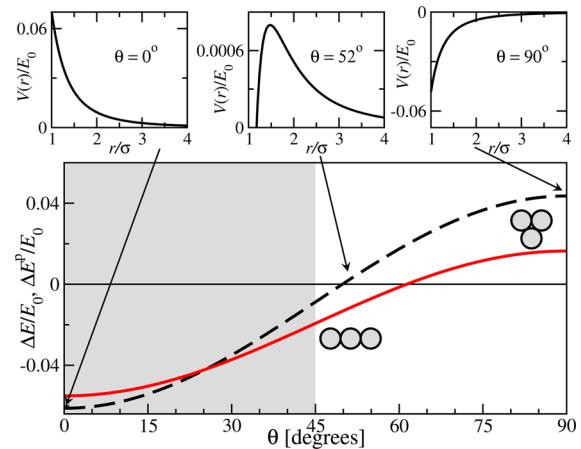


Figure 3. Comparison of the energy difference $\Delta E \equiv E_{\text{ch}} - E_{\text{tr}}$ between chain and triangular clusters of three particles for pairwise additive potentials (black dashed line) and for the full many-body interactions (red solid line). The shaded region depicts the range of $\theta < 45^\circ$ where the pair interactions are purely repulsive and clusters are not stable against hexagonal crystalline arrangement. For $\theta > 45^\circ$, the triangular configuration is the stable one when $\Delta E > 0$, whereas chains prevail in the regions where $\Delta E < 0$.

of the two three-particle configurations E_{ch} and E_{tr} in two ways: (1) By assuming pairwise additivity of the energy: $E_{\alpha}^{\text{p}}(\mathbf{r}_1, \mathbf{r}_2, \mathbf{r}_3) - 3E_0/2 = V(r_{12}) + V(r_{13}) + V(r_{23})$, where $\alpha = \text{ch, tr}$ and $V(r_{ij})$ are the pair interactions between colloids i and j evaluated in the previous step. We obtain for the chains $E_{\text{ch}}^{\text{p}} - 3E_0/2 = 2V(\sigma) + V(2\sigma)$ and for the triangles $E_{\text{tr}}^{\text{p}} - 3E_0/2 = 3V(\sigma)$; therefore, the energy difference between the two arrangements in this pairwise additivity approximation is given as $\Delta E^{\text{p}} \equiv E_{\text{ch}}^{\text{p}} - E_{\text{tr}}^{\text{p}} = V(2\sigma) - V(\sigma)$. (2) By self-consistently solving eqs 2 and 4 for three particles, a procedure which correctly incorporates the three-body interaction terms.

The resulting energy differences from the two approaches above are shown in Figure 3. It is evident that the omission of the three-body interaction terms leads to qualitatively wrong structural predictions: in the range of θ where clusters are expected to form (roughly the nonshaded region in Figure 3), the pairwise picture predicts triangular clusters, while the three-body terms, consistent with the experimental observations (Figure 2), stabilize the chains for a wide parameter range of $\theta \lesssim 62^\circ$. The three-body interaction terms are anisotropic and create a lateral barrier around a colloidal dimer (see Figure 5 and ref 27), so the third particle attaches along the axis and

forms a short chain. A correct description of the full N -body problem, therefore, would require the self-consistent evaluation of the local fields and magnetizations for any arbitrary particle configuration, a procedure which is computationally very involved and includes, in principle, the whole hierarchy of N -body forces in the problem. It would be advantageous to have an effective, physically informed pairwise-additive description of the system by means of a model of interactions that are capable of reproducing the experimental results with high accuracy. This endeavor is the subject of the following section.

4. INVERSE ENGINEERING

In the past decades, computer simulations have proven to be an extremely reliable tool for predicting and analyzing the structural and dynamical properties of various colloidal systems, ranging from hard spheres to more complex structures such as polymers³⁸ and bioproteins.^{39,40} Such simulations often rely on effective pair potentials, which are obtained by tracing out superfluous degrees of freedom while still retaining the key features of the system. However, as demonstrated above, the strong and anisotropic many-body effects in the presented experimental system make it conceptually difficult (if not impossible) to construct effective isotropic and state-independent potentials using approaches that rely on the pairwise additivity of the interactions. This is a major problem even for systems with weaker many-body effects, such as charged colloidal suspensions,⁴¹ since the effective (isotropic) interactions depend not only on the colloidal density but also on the exact arrangement of colloids at a given density.

Therefore, a different concept is called for regarding the theoretical modeling of the systems at hand. In this contribution, we approach the problem from a phenomenological, physically informed, top-down perspective, whereby we carefully engineer effective pair interactions that quantitatively reproduce the experimentally observed structures in the range of the opening angles $0 \leq \theta \leq \theta_m$. On the basis of the experimental facts regarding structure formation, see Figure 2, we argue that the anisotropy introduced by the many-body interactions has a qualitatively similar effect on the macroscopic structures as if the colloidal particles were patchy, i.e., decorated with well-localized interaction sites on their surfaces (see Figure 4). Furthermore, two types of particles can be identified: free, unconnected colloids (type I for isotropic) and colloids forming

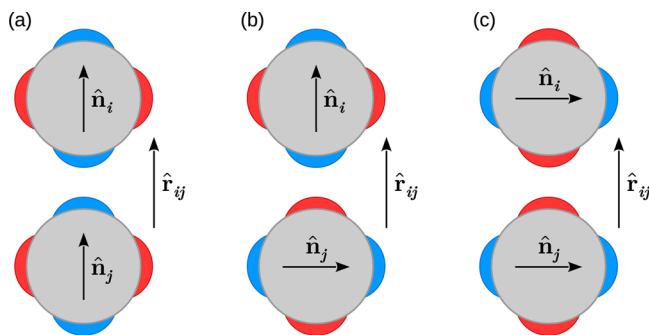


Figure 4. Three exemplary orientations of patchy particles, with two attractive (blue) and two repulsive (red) sites at diametrically opposite sides of the colloids. (a) $\hat{n}_i \parallel \hat{r}_{ij}$ and $\hat{n}_j \parallel \hat{r}_{ij}$, the particles experience the maximum attraction. (b) $\hat{n}_i \perp \hat{r}_{ij}$ and $\hat{n}_j \perp \hat{r}_{ij}$, the particles experience only the isotropic force. (c) $\hat{n}_i \perp \hat{r}_{ij}$ and $\hat{n}_j \perp \hat{r}_{ij}$, the particles feel the maximum repulsion.

chains (type P for patchy). At small opening angles θ of the magnetic field, predominantly type I particles are observed, while at intermediate values below θ_m both types coexist, where the chains form percolated networks with free colloids in the interstitial pockets. For values of $\theta > \theta_m$, only type P colloids trapped in the percolated network are present.

Accordingly, we model the experimental system by introducing an effective mixture of particles I and P and denote the fraction of patchy particles as $\Pi = N_p/N$, where $N \equiv N_p + N_I$ is the total number of colloids in the system. We expect that the ratio between the number of isotropic and patchy colloids strongly correlates with the opening angle θ , in particular, $\Pi = 0$ at $\theta = 0$ and $\Pi = 1$ for $\theta \geq \theta_m$. The effective pair potential $V(1, 2)$ between two particles at positions $\mathbf{r}_i, \mathbf{r}_j$ and orientations $\hat{\mathbf{n}}_i, \hat{\mathbf{n}}_j$ (if patchy) is modeled as follows

$$V(12) = V_{\text{LJ}}(r_{ij}) + \begin{cases} \frac{A_p}{(r_{ij}/\sigma)^3} + \frac{\epsilon_p}{(r_{ij}/\sigma)^6} V_p(\hat{\mathbf{r}}_{ij}, \hat{\mathbf{n}}_i, \hat{\mathbf{n}}_j) & \text{if } i, j \text{ patchy} \\ \frac{A}{(r_{ij}/\sigma)^3} & \text{else} \end{cases} \quad (6)$$

where the first term V_{LJ} is the standard Lennard-Jones potential modeling the impermeability of the particles

$$V_{\text{LJ}}(r_{ij}) = 4\epsilon_{\text{LJ}} \left[\left(\frac{\sigma}{r} \right)^{12} - \left(\frac{\sigma}{r} \right)^6 \right] \quad (7)$$

The second term on the right-hand side of eq 6 represents the repulsive dipolar potential between particles that leads to hexagonal ordering for $\theta \rightarrow 0$. The two isotropic terms describe the interactions involving isotropic particles (I–I and I–P), while the interactions between two patchy particles are characterized by an additional anisotropic patchy potential V_p . The functional dependence of this term is $\sim r^{-6}$. It is physically reasonable to assume two different prefactors $A_p \neq A$ depending on whether the interacting particles are both patchy since the isotropic particles are modeled as experiencing only the perpendicular z component of the magnetic field.

In our model, each patchy colloid has two repulsive and two attractive patches, which are placed on diametrically opposite sides of the colloid, as schematically depicted in Figure 4. We describe the orientation of each particle in the laboratory frame of reference via the unit vector $\hat{\mathbf{n}}_i$, which connects the two attractive patches. Here, it is noteworthy that the patchy particles are constructed in such a way that symmetry $\hat{\mathbf{n}}_i = -\hat{\mathbf{n}}_j$ is obeyed. The anisotropic interaction potential is thus given by $V_p = V_{\text{attr}}(\hat{\mathbf{r}}_{ij}, \hat{\mathbf{n}}_i, \hat{\mathbf{n}}_j) + V_{\text{rep}}(\hat{\mathbf{r}}_{ij}, \hat{\mathbf{n}}_i, \hat{\mathbf{n}}_j)$, where the functional forms of the two contributions are given by

$$V_{\text{attr}} = -[\exp(-\alpha_p \varphi^d) + \exp(-\alpha_p(\varphi - \pi)^d)] (\hat{\mathbf{n}}_i \cdot \hat{\mathbf{r}}_{ij})^2 (\hat{\mathbf{n}}_j \cdot \hat{\mathbf{r}}_{ij})^2 \quad (8)$$

and

$$V_{\text{rep}} = \frac{3}{2} [(\hat{\mathbf{n}}_i \cdot \hat{\mathbf{r}}_{ij})^2 (\hat{\mathbf{n}}_j \cdot \hat{\mathbf{r}}_{ij})^2 - 1] (\hat{\mathbf{n}}_i \cdot \hat{\mathbf{n}}_j)^2 \quad (9)$$

Here, $\varphi = \cos^{-1}(\hat{\mathbf{n}}_i \cdot \hat{\mathbf{n}}_j)$ denotes the relative angle between the attractive patch orientations of two P-type colloids i and j . The patchy particles experience maximum attraction if $\varphi = 0$ or $\varphi = \pi$ and at the same time $\hat{\mathbf{n}}_i \parallel \hat{\mathbf{r}}_{ij}$. If $\hat{\mathbf{n}}_i \perp \hat{\mathbf{r}}_{ij}$, then the attractive potential is zero. The two parameters α_p and d regulate how broad the attractive patches are, and they thus pertain to the architecture of the patchy particles, not to their physical

properties and interaction strengths. The quantity α_p determines the sharpness of the crossover between the patchy regime and the isotropic one on the surface of the colloid, whereas d determines the flatness of the patch–patch interaction. In particular, the crossover becomes sharper with increasing α_p , while high values of d lead to a flattening of the patched regions. Particles that interact solely through these attractive patches preferably arrange in parallel lines. Therefore, in order to construct a reasonable potential landscape around a pair of particles, additional repulsive patches are needed. The repulsive contribution, V_{rep} , leads to a sensitivity on φ in the case of $\hat{\mathbf{n}}_{ij} \perp \hat{\mathbf{r}}_{ij}$. If $\varphi = 0$ or π , then the particles experience the maximum repulsion. The repulsive contribution vanishes for $\varphi = \pi/2$ as well as in the case of $\hat{\mathbf{n}}_{ij} \parallel \hat{\mathbf{r}}_{ij}$. Figure 4 shows a schematic example of three different orientations of patchy particles.

In Figure 5, we show a comparison between the potential landscapes around two adjacent colloids retrieved by (a) self-

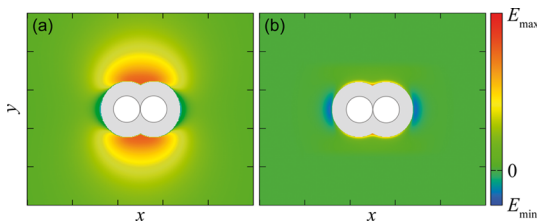


Figure 5. (a) Many-body energy landscape around a pair of magnetic colloids for $\theta = 46^\circ$ and $B_0 = 2.5$ mT. (b) Energy landscape around a pair of patchy particles obtained by the effective pair interactions with $\Pi = 0.96$, $A_p = 15k_B T$, and $\varepsilon_p = 21k_B T$. The gray area corresponds to energy values above E_{max} due to steric effects.

consistently solving the many-body interactions described by eqs 2–5 and (b) using the effective pair potential postulated in eq 6. In the case of the magnetic colloids, a very strong and long-ranged lateral barrier around the colloidal dimer emerges due to many-body effects, which leads to the preferential formation of chains. In comparison, the effective potential has a considerably shorter range, leading to only a very thin repulsive layer, which, on its own, would not be sufficient to drive the formation of chains. Instead, the preferential chain formation is driven by the attractive patches, which are exposed along the x axis. Indeed, we found that the proposed effective interaction is capable of reproducing not only the correct structural properties but also the dynamics of the original system.

Equation 6, in conjunction with eqs 8 and 9, leads to a large parameter space (ε_{LJ} , A , A_p , ε_p , α_p , d , and the ratio Π) that has to be explored to determine a suitable mapping. From the experiments, the radial distribution functions $g(r)$ have been evaluated at density $\rho\sigma^2 = 0.165$ for three values of the opening angle, namely, $\theta = 39$, 46 , and 59° . We used these functions as the criterion to quantify the quality of our model predictions. At this point, we emphasize that it is highly nontrivial to reproduce the typical patterns, number of neighbors, or even dynamics by matching the radial distribution functions, which is a strongly averaged quantity, from experiments and simulations.

To find the optimal values for the parameters, we used a genetic algorithm (GA) combined with Monte Carlo (MC) simulations: at each step, a new set of parameter values was determined by the GA, and then MC simulations were performed to evaluate the $g(r)$ (further details in the Appendix). This procedure was then repeated until we found

a good agreement between the $g(r)$ from experiments and simulations. In addition, we also checked visually whether the final structures shared qualitative features with the experiment.

Although it is generally possible to apply this approach to determine all seven free parameters for every single state point, such an endeavor would be neither satisfactory in principle nor always feasible in practice due to the sheer number of parameter combinations. It is advantageous to proceed with a physically informed approach which a priori recognizes those parameters that should have a dependence on the opening angle θ of the field and, possibly, on the density of the ensemble and treats them separately from those that should not. In this way, the parameter space is reduced prior to performing the optimization.

Our reference state is the one with colloidal density $\rho_{\text{ref}} = \rho\sigma^2 = 0.165$ and the smallest opening angle for which nontrivial patterns are obtained in the experiment, i.e., $\theta = 39^\circ$. We then used the GA to determine the values of all seven model parameters at this state point, which were subsequently fine-tuned by hand. We ensured that the obtained parameters resulted in the best matching between experiments and simulations by restarting the GA with the optimized parameters and indeed did not find any further improvement. As the parameters ε_{LJ} , A , α_p , and d refer to generic steric repulsions (ε_{LJ}), isotropic–isotropic interactions (A), and the patchy particle architecture (α_p and d), we postulate that these are independent of both the opening angle and the density of the system. In this way, the search space of the problem is reduced from having to find seven parameters to three, namely, A_p , ε_p , and Π . At the same time, on physical grounds, we know what to expect for the variation of these three with the opening angle θ at a fixed colloidal density $\rho\sigma^2$. At $\theta = 0$, only the dipolar interaction term is present; therefore, $\Pi(\theta = 0) = 0$. At $\theta = \theta_m$, the dipolar term should vanish, resulting in $A_p(\theta_m) = 0$ and $\Pi(\theta_m) = 1$. Moreover, we surmise that both A_p and ε_p are decreasing monotonically with increasing θ . We then employed the GA to determine the remaining three θ -dependent parameters $A_p(\theta)$, $\varepsilon_p(\theta)$, and $\Pi(\theta)$ from the available experimental data, with the fulfillment of the above physical expectations serving as an additional test of the validity of our approach. Finally, we used linear interpolation to determine A_p , ε_p , and Π at intermediate θ values.

In the experiments, we have used video microscopy and custom-made particle recognition software to characterize the patterns by evaluating the radial distribution function and the nearest-neighbors statistics. By employing the aforementioned mapping procedure for the case $\theta = 39^\circ$, we found that in order to reproduce the observed phases and especially the Y junctions at higher θ values, the attractive patches need to be relatively broad. Therefore, we fixed the values to $\alpha_p = 1.5$ and $d = 8$. The depth of the Lennard-Jones potential was set to the value $\varepsilon_{\text{LJ}} = 55k_B T$, while the strength of the dipolar repulsion was set to $A = 100k_B T$. As mentioned before, these values were kept fixed for all other combinations of the opening angle of the field and the colloidal density. Here, we found that our results were most sensitive to changes to the energy scales, i.e., A and ε_{LJ} , while changes to the patch geometry (through α_p and d) had a smaller impact on the emerging structures. In general, our results were robust with respect to (small) fluctuations of these four fixed parameters, since the GA attempts to optimize the remaining free parameters accordingly to match the $g(r)$.

Using the GA, we found $\Pi = 0.06$, $A_p = 78k_B T$, and $\varepsilon_p = 57k_B T$ for the θ -dependent values at the opening angle $\theta = 39^\circ$

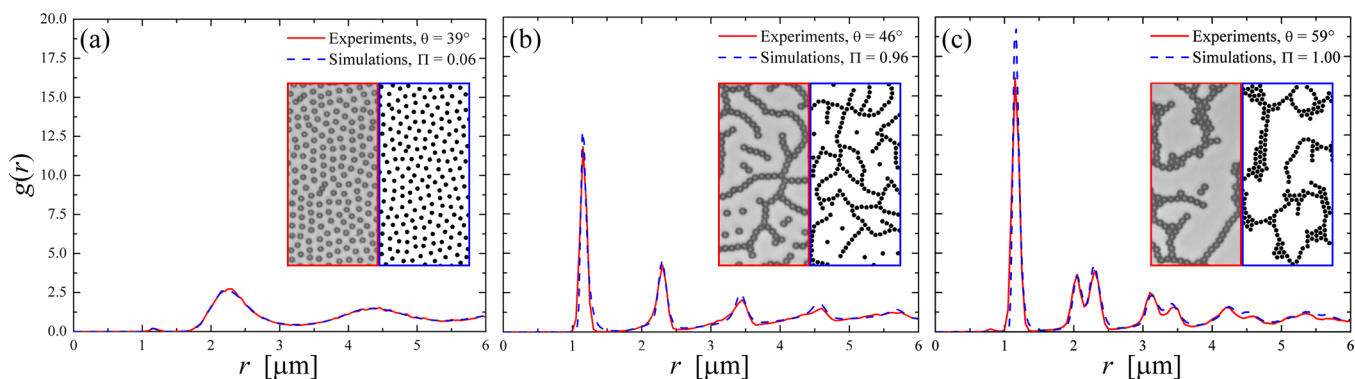


Figure 6. Radial pair distribution function $g(r)$ obtained from experiments (solid red lines) and simulations (dashed blue lines). The insets show representative snapshots from the experimental systems (left half) and from the model systems (right half). Results are shown for opening angles $\theta = 39, 46,$ and 59° , and the respective values of Π , namely, $\Pi = 0.06, 0.96,$ and 1.00 . The density is fixed at the value $\rho\sigma^2 = 0.165$.

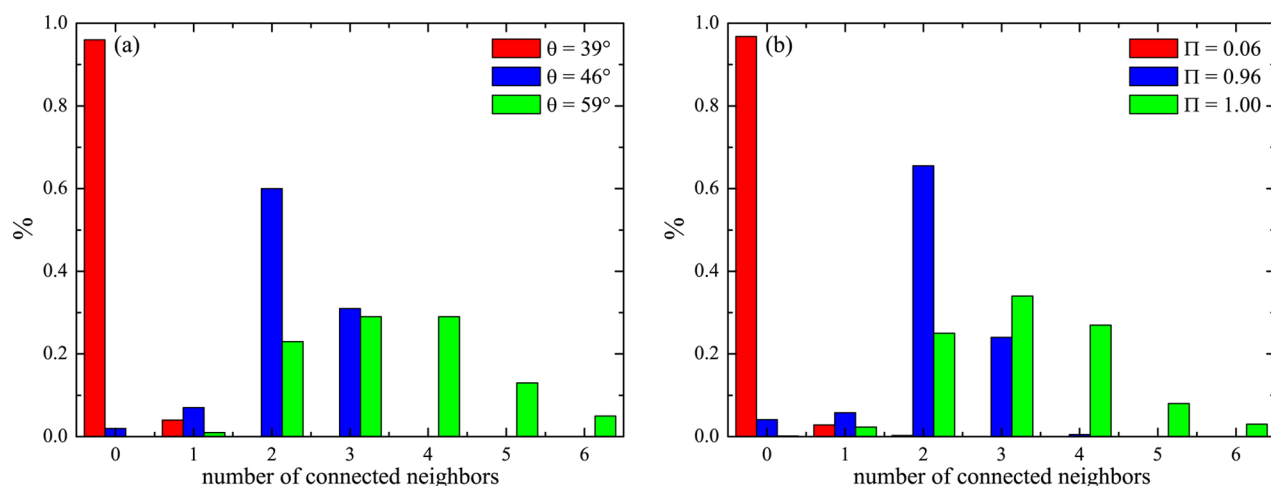


Figure 7. Distribution of the number of nearest neighbors extracted from (a) experiments and (b) simulations.

at density $\rho\sigma^2 = 0.165$. For the case $\theta = 46^\circ$, we found $\Pi = 0.96$, $A_p = 15.0k_B T$, and $\varepsilon_p = 21k_B T$. These results are consistent with the theoretical prediction of $\Pi = 1.0$ and $A_p = 0.0$ at the magic angle $\theta = \theta_m \approx 54.7^\circ$. For opening angles beyond θ_m , the colloidal particles become purely attractive (hence $A_p < 0$). Moreover, the θ -dependence of the parameters A_p and ε_p vanishes, since Π does not increase anymore. In this range, we found that the experimental results could be matched the best using $A_p = -k_B T$ and $\varepsilon_p = 15.2k_B T$.

The quality of the inverse-engineering procedure at this fixed density is judged by a comparison between the theoretical and experimental radial distribution functions $g(r)$ as well as the characteristic configuration snapshots of the system. This comparison is shown in Figure 6. The excellent agreement between the radial distribution functions offers strong support to our approach, yet one could argue that this is expected, since it is precisely the minimization of the integral of the absolute value of their difference that is aimed for in our approach. However, the $g(r)$ is a rotationally averaged quantity and agreement between theory, and the experiment between the two offers no guarantee for a matching between typical configurations. In this sense, the remarkable agreement between experimental and theoretical snapshots of the system at all opening angles, as shown in the insets of Figure 6, offers strong corroboration of the reliability of our approach.

To quantify further the local coordination of the investigated systems, we performed a neighbor analysis of the emerging

patterns where we counted the number of nearest neighbors for each colloid. A comparison between the results from experiments and simulations is shown in Figure 7, demonstrating once again the excellent quantitative agreement between them. These data show that a vast majority of particles were isolated at small opening angles θ and correspondingly small fractions Π . As the angle is slowly increased, the particles assemble to chains and Y junctions, which is reflected in the large peaks for two and three neighbors. For $\theta \geq \theta_m$, frothlike structures emerged, leading to a relatively broad distribution of nearest neighbors.

Until now, the comparison has been performed for a fixed colloidal density. It has to be determined which of the model parameters are expected to depend on concentration and in which fashion. Consistently with the aforementioned philosophy, we leave parameters A , ε_{Lj} , α_p , and d untouched and we focus on A_p , ε_p , and Π . To further restrict the (apparent) freedom in their choice, we refer again to physical arguments. These three parameters encode the many-body effects which arise due to the depolarization effects on any given colloid for all of the other colloids in the system. As this effect is due to the long-range dipolar interaction, we surmise that it can be taken into account in a mean-field fashion and thus that the free parameters will scale linearly with density for any given opening angle θ . Accordingly, we postulate the following density dependence, introducing a constant scaling parameter λ_p :

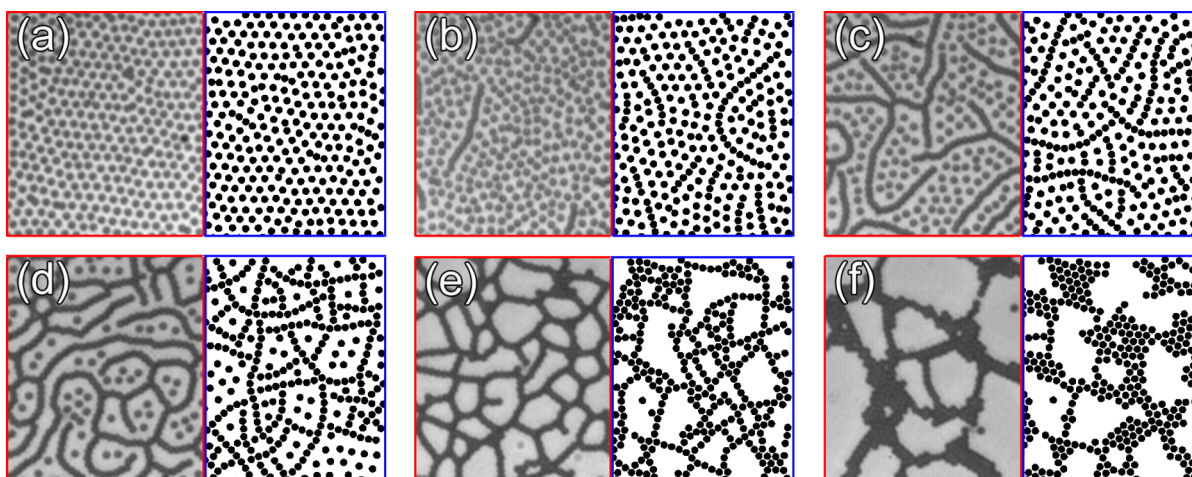


Figure 8. Typical system configurations for $\rho\sigma^2 = 0.33$ from experiments (left half) and simulations (right half). (a) $\theta = 41^\circ$ and $\Pi = 0.16$, (b) $\theta = 44^\circ$ and $\Pi = 0.36$, (c) $\theta = 46^\circ$ and $\Pi = 0.56$, (d) $\theta = 48^\circ$ and $\Pi = 0.86$, (e) $\theta = 55^\circ$ and $\Pi = 1.0$, and (f) $\theta = 90^\circ$ and $\Pi = 1.0$.

$$A_p(\rho) = \left[1 + \lambda_p(\rho - \rho_{\text{ref}})/\rho_{\text{ref}} \right] A_p(\rho_{\text{ref}}) \quad (10)$$

and

$$\varepsilon_p(\rho) = \left[1 + \lambda_p(\rho - \rho_{\text{ref}})/\rho_{\text{ref}} \right] \varepsilon_p(\rho_{\text{ref}}) \quad (11)$$

The GA-search for $\rho \neq \rho_{\text{ref}}$ thus proceeds as follows. With the functional dependence $A_p(\Pi)$ and $\varepsilon_p(\Pi)$ acquired at the density ρ_{ref} we first rescale these functions according to eqs 10 and 11 above. This leaves us, for an arbitrary density $\rho \neq \rho_{\text{ref}}$ with just two unknown parameters, $\Pi(\theta)$ and the prefactor λ_p above, which we take to be θ -independent. With the choice $\lambda_p = 0.6$, our approach yields now, also at a different density $\rho\sigma^2 = 0.33$, patterns that strongly resemble the ones observed in the experiments, as shown in Figure 8.

Finally, we also performed a qualitative study of the short-time dynamics of both the experimental and the model systems. Figure 9(a) shows a color-coded snapshot of the experimental system, which was obtained by overlapping 10 consecutive snapshots separated by 0.1 s, and it is very visible that we can distinguish between two different types: particles constituting the percolating network move only barely over the course of the image capture (1 s) while the free colloids and particles at

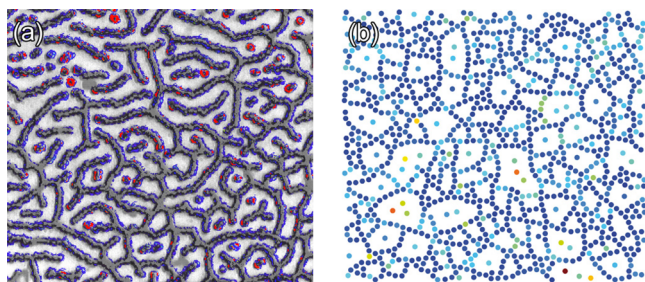


Figure 9. Relative mobility of colloids obtained from (a) experiments by overlapping 10 consecutive snapshots with a time step of 100 ms and (b) simulations by measuring the mean-square displacement of each particle. Experiments and simulations have been conducted at $\rho\sigma^2 = 0.33$ and a field opening angle of $\theta = \theta_m$. Particles colored in blue exhibit no or very little mobility, while particles colored in red have a relatively large mobility. Note that the free colloids and the dangling chain ends clearly move more than the colloids forming the percolating mesh.

the chain ends exhibit a significantly higher mobility. These inhomogeneous dynamics are nicely reproduced in the model system as illustrated in Figure 9. In the simulations, the patchy particles form the percolating mesh and are therefore frustrated in their motion, while the remaining isotropic particles can move in the voids of the network. This qualitative agreement between experiments and simulations is remarkable, since we used only static properties, i.e., the radial pair distribution function $g(r)$, to determine the model parameters.

5. CONCLUSIONS

We studied the collective ordering of superparamagnetic colloids confined to 2D and driven by a high-frequency precessing external magnetic field. In the experiments, we observed a rich sequence of quasi-equilibrium structures as we varied the parameters of the external field. The theoretical description of the system is challenging due to the complex depolarization effects. The observed structures could not be reproduced by simple isotropic density-dependent effective pair interactions. On the basis of the insights from many-body calculations, we postulated a coarse-grained model that is a binary mixture of patchy and nonpatchy particles with effective anisotropic pair interactions. By adjusting the mixture composition, we modeled different opening angles of the external magnetic field. We then employed a heuristic optimization scheme based on genetic algorithms in conjunction with Monte Carlo simulations to determine the model parameters by matching selected radial distribution functions from experiments and simulations. This physically informed coarse-graining approach has been inspired by the particular pattern formation in the experiments. However, the idea of modeling many-body effects via mixtures of patchy and isotropic particles is general; therefore, our method can be transferred to other similar problems by adjusting the model parameters. Following this route, we achieved quantitative agreement between the colloidal structures in the experiments and simulations. Moreover, even though the effective potentials were derived from purely static quantities, the coarse-grained model qualitatively reproduced also the colloidal dynamics: in the region of parameters where percolated and free colloids coexist, the experiments and simulations show dynamic heterogeneity. In addition, we found that the wall-clock simulation time for the coarse-grained systems was about 2

orders of magnitude shorter than for the self-consistent solution. Hence, we conclude that the effective pair potentials of our model can be used in conjunction with conventional simulation methods to predict structural and dynamical system properties. In particular, our proposed method allows for studying the structure factor at low wavelengths, providing information on thermodynamic properties of the system, which are difficult to retrieve through experiments.

■ APPENDIX: GENETIC ALGORITHM

The genetic algorithm was originally developed by John Holland⁴² in the 1970s and since then has also achieved high popularity in the realm of soft matter physics.^{23,43–45} As the naming suggests, this heuristic optimization method mimics the fundamental principles of biological evolution, i.e., selection, recombination, and mutation, to find the best solution. Following this nomenclature, we will refer to each possible solution as an individual \mathcal{I} , where every individual \mathcal{I} contains a chromosome which holds the parameter set in a binary representation b_i .

In our implementation, every free simulation parameter (A_p , ϵ_p , and Π) has a corresponding binary representation b_i , where each b_i is a sequence of 32 elements from a binary alphabet $\mathcal{A} \in \{0, 1\}$. We then interpret each b_i as a 32 bit fixed-point variable, with values ranging from 0 to 1 in steps of $2^{-32} \approx 10^{-10}$. Hence, each individual is described by $|\mathcal{I}| = 96$ genes. This binary representation of the parameters is the so-called genotype, which corresponds to a point in search space and hence one candidate solution (phenotype). We can then translate any given b_i to its corresponding simulation parameter by multiplying by its upper bound ($A_p^{\max} = 100k_B T$ and $\epsilon_p^{\max} = 100k_B T$). All N_I individuals belonging to the same iteration are called a generation \mathcal{G}_i .

The individuals of the first generation \mathcal{G}_0 are chosen randomly, where the typical number of individuals comprising one generation is typically $N_I = 40$. Every individual is associated with a so-called fitness, which quantifies the quality of the represented solution. As outlined in section 4, we employ the deviation from the experimental radial distribution function, $g_e(r)$, as our quality indicator. Thus, the fitness function is given by

$$f(\mathcal{I}) = \exp\left(-\int \lg(r) - g_{\text{exp}}(r) | dr\right) \quad (12)$$

It is readily visible that the fitness of an individual approaches 1 if the $g(r)$ from the simulations is close to the experimental findings and that $f(\mathcal{I}) \rightarrow 0$ for large discrepancies. After all \mathcal{I} individuals of one generation \mathcal{G}_i are examined, the subsequent generation \mathcal{G}_{i+1} is populated by new individuals. In this process, the best individual from the previous generation is transferred unaltered to the new generation (elitism), while the remainder of the population is created by performing one-point crossovers on the genetic material of the two parents. The latter are chosen with probabilities proportional to their fitness values, namely,

$$p(\mathcal{I}) = \frac{f_{\mathcal{I}}}{\sum_{\mathcal{I} \in \mathcal{G}_i} f(\mathcal{I})} \quad (13)$$

Such a selection mechanism is often referred to as a Roulette-wheel selection. After two parents are chosen, the chromosomes of these two individuals have to be recombined.

Therefore, a cutting point is randomly selected at which the chromosomes are sliced and merged into a new chromosome. Thus, this recombination step is completely blind to the underlying representation of the parameters, as it can dissect a b_i .

In the next step, point mutations are performed, i.e., arbitrary bits in the chromosomes are flipped from 0 to 1 and vice versa. This procedure is of utmost importance to increasing the genetic diversity by introducing new or lost information into the system, and the probability for each mutation is typically 1 to 2%. This cycle is then repeated until the model parameters converge, which was typically the case after about 20 generations. Finally, we take the results obtained by the GA and optimize them via a hill-climbing algorithm.

■ AUTHOR INFORMATION

Corresponding Authors

*E-mail: jd489@cam.ac.uk

*E-mail: arashn@princeton.edu

Notes

The authors declare no competing financial interest.

■ ACKNOWLEDGMENTS

This work was supported by the Seventh Framework Programme of the European Union through grants ARG-ERC-COLSTRUCTION 227758 and ITN-COMPLOIDS 234810, by the Slovenian Research Agency through grant P1-0055, and the Princeton Center for Complex Materials (PCCM), a U.S. National Science Foundation Materials Research Science and Engineering Center (grant DMR-0819860).

■ REFERENCES

- (1) Li, F.; Josephson, D. P.; Stein, A. Colloidal assembly: the road from particles to colloidal molecules and crystals. *Angew. Chem., Int. Ed.* **2011**, *50*, 360–388.
- (2) Law, A. D.; Buzza, D.; Horozov, T. S. Two-dimensional colloidal alloys. *Phys. Rev. Lett.* **2011**, *106*, 128302.
- (3) Law, A. D.; Auriol, M.; Smith, D.; Horozov, T. S.; Buzza, D. Self-assembly of two-dimensional colloidal clusters by tuning the hydrophobicity, composition, and packing geometry. *Phys. Rev. Lett.* **2013**, *110*, 138301.
- (4) Weddemann, A.; Wittbracht, F.; Eickenberg, B.; Hütten, A. Magnetic Field Induced Assembly of Highly Ordered Two-Dimensional Particle Arrays. *Langmuir* **2010**, *26*, 19225–19229.
- (5) Leunissen, M. E.; Vutukuri, H. R.; van Blaaderen, A. Directing colloidal self-assembly with biaxial electric fields. *Adv. Mater.* **2009**, *21*, 3116–3120.
- (6) Ristenpart, W. D.; Aksay, I. A.; Saville, D. A. Electrically guided assembly of planar superlattices in binary colloidal suspensions. *Phys. Rev. Lett.* **2003**, *90*, 128303.
- (7) Khalil, K. S.; Sagastegui, A.; Li, Y.; Tahir, M. A.; Socolar, J. E. S.; Wiley, B. J.; Yellen, B. B. Binary colloidal structures assembled through Ising interactions. *Nat. Commun.* **2012**, *3*, 794.
- (8) Nych, A.; Ognysta, U.; Škarabot, M.; Ravnik, M.; Žumer, S.; Muševič, I. Assembly and control of 3D nematic dipolar colloidal crystals. *Nat. Commun.* **2013**, *4*, 1489.
- (9) Mangold, K.; Leiderer, P.; Bechinger, C. Phase Transitions of Colloidal Monolayers in Periodic Pinning Arrays. *Phys. Rev. Lett.* **2003**, *90*, 158302.
- (10) Mikhael, J.; Roth, J.; Helden, L.; Bechinger, C. Archimedean-like tiling on decagonal quasicrystalline surfaces. *Nature* **2008**, *454*, 501–504.
- (11) Dotera, T.; Oshiro, T.; Zihler, P. Mosaic two-lengthscale quasicrystals. *Nature* **2014**, *506*, 208–211.

- (12) Demirörs, A. F.; Pillai, P. P.; Kowalczyk, B.; Grzybowski, B. A. Colloidal assembly directed by virtual magnetic moulds. *Nature* **2013**, *503*, 99–103.
- (13) Bianchi, E.; Likos, C. N.; Kahl, G. Self-assembly of heterogeneously charged particles under confinement. *ACS Nano* **2013**, *7*, 4657–4667.
- (14) van Blaaderen, A.; Ruel, R.; Wiltzius, P. Template-directed colloidal crystallization. *Nature* **1997**, *385*, 321–324.
- (15) Louis, A. A. Beware of density dependent pair potentials. *J. Phys.: Condens. Matter* **2002**, *14*, 9187.
- (16) Likos, C. N. Effective interactions in soft condensed matter physics. *Phys. Rep.* **2001**, *348*, 267–349.
- (17) Zahn, K.; Lenke, R.; Maret, G. Two-stage melting of paramagnetic colloidal crystals in two dimensions. *Phys. Rev. Lett.* **1999**, *82*, 2721–2724.
- (18) Zahn, K.; Maret, G.; Russ, C.; von Grünberg, H. H. Three-particle correlations in simple liquids. *Phys. Rev. Lett.* **2003**, *91*, 115502.
- (19) Eisenmann, C.; Gasser, U.; Keim, P.; Maret, G. Anisotropic defect-mediated melting of two-dimensional colloidal crystals. *Phys. Rev. Lett.* **2004**, *93*, 105702.
- (20) Eisenmann, C.; Gasser, U.; Keim, P.; Maret, G.; von Grünberg, H. H. Pair interaction of dislocations in two-dimensional crystals. *Phys. Rev. Lett.* **2005**, *95*, 185502.
- (21) Hoffmann, N.; Ebert, F.; Likos, C. N.; Löwen, H.; Maret, G. Partial clustering in binary two-dimensional colloidal suspensions. *Phys. Rev. Lett.* **2006**, *97*, 078301.
- (22) Osterman, N.; Babič, D.; Poberaj, I.; Dobnikar, J.; Zihler, P. Observation of Condensed Phases of Quasipolar Core-Softened Colloids. *Phys. Rev. Lett.* **2007**, *99*, 248301.
- (23) Dobnikar, J.; Fornleitner, J.; Kahl, G. Ground states of model core-softened colloids. *J. Phys.: Condens. Matter* **2008**, *20*, 494220.
- (24) Fornleitner, J.; Lo Verso, F.; Kahl, G.; Likos, C. N. Genetic algorithms predict formation of exotic ordered phases for two-dimensional dipolar monolayers. *Soft Matter* **2008**, *4*, 480–484.
- (25) Chremos, A.; Likos, C. N. Crystal structures of two-dimensional binary mixtures of magnetic colloids in titled external fields. *J. Phys. Chem. B* **2009**, *113*, 12316–12325.
- (26) Tierno, P.; Muruganathan, R.; Fischer, T. M. Viscoelasticity of dynamically self-assembled paramagnetic colloidal clusters. *Phys. Rev. Lett.* **2007**, *98*, 028301.
- (27) Osterman, N.; Poberaj, I.; Dobnikar, J.; Frenkel, D.; Zihler, P.; Babič, D. Field-Induced Self-Assembly of Suspended Colloidal Membranes. *Phys. Rev. Lett.* **2009**, *103*, 228301.
- (28) Martin, J. E.; Anderson, R. A.; Tigges, C. P. Thermal coarsening of uniaxial and biaxial field-structured composites. *J. Chem. Phys.* **1999**, *110*, 4854.
- (29) Martin, J. E.; Venturini, E.; Gulley, G. L.; Williamson, J. Using triaxial magnetic fields to create high susceptibility particle composites. *Phys. Rev. E* **2004**, *69*, 021508.
- (30) Snezhko, A.; Aranson, I. S.; Kwok, W.-K. Surface Wave Assisted Self-Assembly of Multidomain Magnetic Structures. *Phys. Rev. Lett.* **2006**, *96*, 078701.
- (31) Snezhko, A.; Belkin, M.; Aranson, I. S.; Kwok, W.-K. Self-Assembled Magnetic Surface Swimmers. *Phys. Rev. Lett.* **2009**, *102*, 118103.
- (32) Snezhko, A.; Aranson, I. S. Magnetic manipulation of self-assembled colloidal asters. *Nat. Mater.* **2011**, *10*, 698–703.
- (33) Yan, J.; Bloom, M.; Bae, S. C.; Luijten, E.; Granick, S. Linking synchronization to self-assembly using magnetic Janus colloids. *Nature* **2012**, *91*, 578.
- (34) Dobnikar, J.; Snezhko, A.; Yethiraj, A. Emergent colloidal dynamics in electromagnetic fields. *Soft Matter* **2013**, *9*, 3693–3704.
- (35) Martin, J. E.; Anderson, R. A.; Williamson, R. L. Generating strange magnetic and dielectric interactions: Classical molecules and particle foams. *J. Chem. Phys.* **2003**, *118*, 1557–1570.
- (36) Kulic, I. M.; Kulic, M. L. Self-Assembly of Colloidal Superstructures in Coherently Fluctuating Fields. *Phys. Rev. Lett.* **2013**, *111*, 198301.
- (37) Panofsky, W.; Phillips, M. *Classical Electricity and Magnetism*, 2nd ed.; Addison-Wesley: Reading, MA, 1962.
- (38) Müller-Plathe, F. Coarse-graining in polymer simulation: From the atomistic to the mesoscopic scale and back. *ChemPhysChem* **2002**, *3*, 754–769.
- (39) Cornell, W.; Cieplak, P.; Bayly, C.; Gould, I.; Merz, K.; Ferguson, D.; Spellmeyer, D.; Fox, T.; Caldwell, J.; Kollman, P. A 2nd Generation Force-field for the Simulation Of Proteins, Nucleic-Acids, and Organic-Molecules. *J. Am. Chem. Soc.* **1995**, *117*, 5179–5197.
- (40) Case, D. A.; Cheatham, T. E.; Darden, T.; Gohlke, H.; Luo, R.; Merz, K. M.; Onufriev, A.; Simmerling, C.; Wang, B.; Woods, R. J. The Amber biomolecular simulation programs. *J. Comput. Chem.* **2005**, *26*, 1668–1688.
- (41) Dobnikar, J.; Chen, Y.; Rzehak, R.; von Grünberg, H. H. Many-body interactions and the melting of colloidal crystals. *J. Chem. Phys.* **2003**, *119*, 4971.
- (42) Holland, J. H. In *Adaptation in Natural and Artificial Systems: An Introductory Analysis with Applications to Biology, Control, and Artificial Intelligence*; Holland, J. H., Ed.; MIT Press: Cambridge, MA, 1975.
- (43) Pauschenwein, G.; Kahl, G. Clusters, columns, and lamellae—minimum energy configurations in core softened potentials. *Soft Matter* **2008**, *4*, 1396–1399.
- (44) Filion, L.; Dijkstra, M. Prediction of binary hard-sphere crystal structures. *Phys. Rev. E* **2009**, *79*, 046714.
- (45) Nikoubashman, A.; Likos, C. N. Self-assembled structures of Gaussian nematic particles. *J. Phys.: Condens. Matter* **2010**, *22*, 104107.